

8-30-2024

## Endwall Contouring for Lowering the Thermal Load and Augmenting the Turbine Efficiency

Arjun Kozhikkatil Sunil

*Division of Mechanical Engineering, School of Engineering, Cochin University of Science & Technology, Kalamassery 682022, India, arjunks@cusat.ac.in*

Tide Porathoor Sunny

*Division of Mechanical Engineering, School of Engineering, Cochin University of Science & Technology, Kalamassery 682022, India, tidepscusat@gmail.com*

Follow this and additional works at: <https://scholarhub.ui.ac.id/mjt>



Part of the [Dynamics and Dynamical Systems Commons](#), and the [Heat Transfer, Combustion Commons](#)

---

### Recommended Citation

Sunil, Arjun Kozhikkatil and Sunny, Tide Porathoor (2024) "Endwall Contouring for Lowering the Thermal Load and Augmenting the Turbine Efficiency," *Makara Journal of Technology*. Vol. 28: Iss. 2, Article 1.

DOI: 10.7454/mst.v28i2.1639

Available at: <https://scholarhub.ui.ac.id/mjt/vol28/iss2/1>

This Article is brought to you for free and open access by the Universitas Indonesia at UI Scholars Hub. It has been accepted for inclusion in Makara Journal of Technology by an authorized editor of UI Scholars Hub.

# Endwall Contouring for Lowering the Thermal Load and Augmenting the Turbine Efficiency

Arjun Kozhikkatil Sunil\* and Tide Porathoor Sunny

Division of Mechanical Engineering, School of Engineering,  
Cochin University of Science & Technology, Kalamassery 682022, India

\*E-mail: arjunks@cusat.ac.in

---

## Abstract

Endwall contouring having significance in delineating ideal endwalls competent in thermal load depletion is the focus of this study. We have successfully utilized non-axisymmetric contoured endwalls to enhance turbine performance by controlling the secondary flow characteristics in a blade passage through steady-state numerical hydrodynamics. The supreme endwall pattern could lower the gross pressure loss at the design stage and is related to the size of the top-loss location being productively lowered. The selective numerical shape change using multi-objective optimization at the most prominent locations resulted in contoured endwall geometry and a considerable reduction of thermal exchange in the vane passage and thermal load in the turbines. A non-axisymmetric contoured endwall achieves the highest net heat flux reduction and elevated aerodynamic performance with lower total pressure loss coefficients than an axisymmetric convergent contoured endwall at most locations of the endwall. In the present study, the ideal mass flow rate could pinpoint the endwall passage, contoured with outstanding axial turbine competence and longevity. Endwall contouring enhances turbine performance, and augmented efficiency is achieved with optimized shapes.

*Keywords: aerodynamic performance, contoured endwall, net heat flux reduction, non-axisymmetric contouring, turbine blade*

---

## 1. Introduction

To attain enhanced effectiveness, the temperature at the entrance of the turbine is enhanced to elevate the temperature of the inlet adjacent to the endwall region, which, in turn, increases the need to cool the endwall region of the nozzle guide vane (NGV). Understanding the impact of two-dimensional (2D) contouring of the endwall on aerodynamic performance and adiabatic cooling effectiveness ( $\eta$ ) is important [1]. Thus, the competency of the thermal circle and the persistence of the gas turbine engine constituents need to be augmented [2]. Controlling secondary flows [3] with a high blowing ratio (BR) has been reported. Subject to the association of an incoming corotating vortex, non-axisymmetric contoured endwall profiling diminished the load on the vane adjacent to the endwall region and cascade loss [4]. High-lift airfoils need more dramatic topography to achieve the best aerodynamic performance [5].

Endwall contouring enhanced both turbulence and thermal exchange ahead of the passage but reduced thermal exchange at the inside region of the passage [6]. One leg of the horseshoe vortex (HV) that develops into

the passage vortex was identified as a main contributor to the endwall losses, followed by the unsteady wakes shed by upstream stages [7]. The non-axisymmetric contoured endwall is adjacent to the blade leading edge, which weakens the HV and lowers the Stanton number [8]. Three-dimensional (3D) non-axisymmetric endwall contouring is particularly used in blades [9], which reduces the profile loss and inhibits the secondary flow of a low-aspect-ratio cascade [10]. Slot coolant coverage for the endwall with a contoured shape was better than that with a flat shape [11].

To enhance the efficiency of gas turbines, the temperature at the entrance of the turbine is elevated. Hence, the thermal loading at the turbine vane is higher, and the secondary losses of the flow happen to be the pertinent part of the performance of the turbine caused by the association between the HV and the powerful cross-flow at the endwall. A local heat transfer increase of 20% adjacent to the passage junction on the pressure side and an overall heat transfer decrease of 3% have been reported for contoured endwalls [12]. The turbomachinery blading effectiveness of 2D airfoils is enhanced by the tangential contouring of the endwall; although the first-

stage effectiveness of interfaces suppresses the positive effects, contouring of the endwall effectively improves the engine gross performance [13].

Contouring could reduce the losses due to secondary flow with the passage location obtaining the most benefit and the upstream airfoil region obtaining the least benefit [14]. The axisymmetric endwall of the contoured geometry of the NGV exhibited bottom-level heat transfer [15], and the enhancement of thermal exchange decreased with an increase in leakage flow [16]. The endwall of the first NGV is a critical portion because of the terrible operating conditions, complicated 3D flow field, and highly exposed area [17]. To protect the endwall from thermal ablation and limit the depletion of compressor bleed air, highly efficient endwall cooling systems are inevitable. Endwall contouring modifies the distribution of static pressure on it by modifying the endwall surface curvature [18], which leads to turbine performance benefits [19]. The secondary losses contribute 30% to 50% of gross losses for a vane with a narrow aspect ratio. All of the optimized endwall designs of contoured geometry identified have recessed areas at the passage central region and an upward area at the passage aft region adjacent to the suction side. A superior thermal exchange performance is attributed to an enhanced heat transfer coefficient (HTC) calculated on a mean area basis with a smaller total endwall area [20]. The performance efficiency of the turbine passage is pivotal to its mid-pitch from the front part to the aft part subjected to stream acceleration [21].

Axisymmetric endwall contouring having prominence in the depiction of advanced endwalls demonstrated substantial depletion of thermal transfer in the vane passage with outstanding axial turbine competence and longevity [22]. Non-axisymmetric endwall contouring resulted in aerodynamic improvements and increased turbine entry temperatures by weakening the interaction between the corner vortex and the tornado-like vortex from the endwall as the main control mechanism [23]. The development of a repetitive and cyclical 3D vortex and its related impact on the local surface thermal exchange processes in the junction region of a turbine vane with a turbulent flow during a forced convection scenario is revealed [24]. A lowered heat load at the endwall region with augmented aerodynamic performance and net heat flux reduction (NHFR) are obtained in the case of an endwall subjected to non-axisymmetric contouring; moreover, the strength of the magnetic field is optimized to reduce the weight and cost of a turbine engine [25].

Multi-objective optimization approach design of the passages of the endwall in a non-axisymmetric manner with the existence of purge flow of the ideal characteristics is developed in this investigation. This study analyzed the endwall regions and shape changes that have a pertinent influence on the thermal exchange of the endwall or the

performance of a passage. The present study is conducted to reduce the endwall heat load of the vane and improve the overall efficiency of the turbine. This study adjudges the optimum contoured shapes based on the axisymmetry and non-axisymmetry of flat-shaped endwalls at an ideal mass flux ratio (MFR). The Nusselt number ( $Nu$ ) distribution in three different endwall shapes is reported and discussed.

The previous heat transfer research on the contouring of the endwall was accomplished with bottom-level outlet Mach numbers, except for enhancing the contouring of the endwall in reducing the turbine passage thermal exchange under the operating conditions of a transonic nature resembling modern engine environments [26]. Experimental evidence on the impact of the contouring of the endwall under transonic leakage flow conditions is unavailable. The purpose of the current investigation is to record outstanding information on the thermal exchange of the contoured endwall in a cascade of turbine blades. At the junction region for a highly contoured endwall, augmented NHFR and aerodynamic performance are the highlights of this study.

## 2. Computational Model and Mesh

The computational domain is the transonic vane cascade with a turbulence intensity of 16% at the inlet, a Reynolds number of  $1.7 \times 10^6$ , a Mach number at the exit, and an upstream purge flow. Figure 1 shows the computational domain of the axisymmetric convergent contoured endwall. The upstream purge flow through 42 cylindrical cooling double-row holes with a diameter of 2.4 mm is considered.

The modeling parameters are selected based on the review of available literature and refined in pilot simulations to lower the thermal load and augment the aerodynamic performance (Figure 2). The capability of coolant flow and its loop of heating/cooling is forced to its operational limits, leading to the struggle of reiterating each situation separately; still, this disruption is nearly absent for every uncooled case. The impact of this disruption on the gross mean thermal exchange provisions does not change the significant interpretations inferred from the outcomes. The coolant distribution across the mainstream is not predominantly elevated because of possible coolant lift-off from the endwall.

A grid independence test was conducted, in which film cooling effectiveness (FCE) distributions around the vane leading edge on the contoured endwall with  $6 \times 10^6$ ,  $9 \times 10^6$ ,  $12 \times 10^6$ , and  $15 \times 10^6$  grid points were compared using the BR 2.5 design. The FCE rating of 0.48 was fixed, as the grid number increased from  $12 \times 10^6$  to  $15 \times 10^6$ . Based on the grid independence analysis, a structure with a mesh size of  $12 \times 10^6$  provides a grid-independent FCE at the endwall. Three different endwall shapes, viz., flat,

axisymmetric (convergent), and non-axisymmetric (shroud with 15% perturbation height to span) contoured endwalls, designed for the first NGV were numerically investigated. An upstream purge flow is contemplated with the holes located  $0.4C_{ax}$  upstream of the blade leading edge in the center passage. Figure 3 shows the axisymmetric contoured endwall mesh. Steady-state RANS with ANSYS FLUENT, pressure–velocity coupling, air, and a realizable  $k-\epsilon$  turbulence model with compressibility, viscous heating, and curvature correction were used.

The  $k-\epsilon$  turbulence model was utilized in many previous studies [27, 28] and recommended as a better option. Alternatively, the SST turbulence design was applied for the identical NGV [29]; however, the outcome was not exceeded in contrast to that in a previous study [28].

Hence, the realizable  $k-\epsilon$  with augmented wall analysis was adopted, as its results have been proven to be greater than those of the standard and other wall functions. Endwall heat transfer augmentation for a non-axisymmetric contour in the passage for the realizable  $k-\epsilon$  turbulence model relative to a flat endwall was relatively consistent with the experiment [6]. Furthermore, the measured and predicted film cooling results using the realizable  $k-\epsilon$  turbulence model indicated that non-axisymmetric contouring limits the distribution of film cooling flow over the endwall depending on the interaction of the film with the contour geometry. The realizable  $k-\epsilon$  turbulence model and the augmented wall procedure were applied, and the compressibility effects, curvature correction, viscous heating effects, and production limiter were accounted for in this model [30].

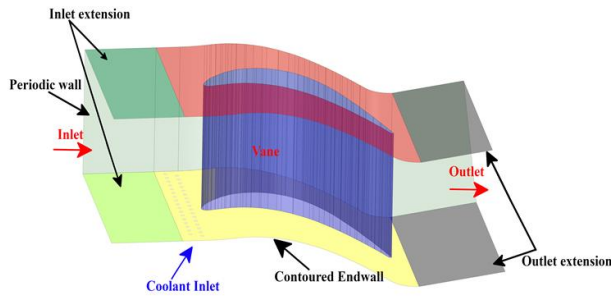


Figure 1. Schematic Diagram of the Linear Vane Cascade

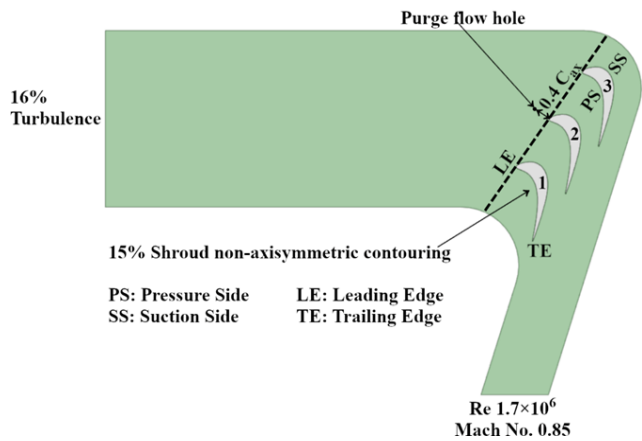


Figure 2. Turbine Vane Endwall Structure with the Selected Modeling Parameters



Figure 3. Mesh Details of the Contoured Vane Endwall

Table 1. Boundary Conditions

Boundary Condition	Value
Inlet mass flow	27 kg/s
Outlet average total pressure	101.325 kPa
Rotation speed	1,500 r/min
Temperature	273 K
Fluid medium	Water

The MFR is expressed as follows:

$$MFR = \frac{\rho_c v_c}{\rho_m v_m}, \quad (1)$$

where  $\rho$  and  $v$  are the density and velocity of coolant and mainstream, respectively. Profiling of the optimum non-axisymmetric endwall contouring with perturbation height to the span of 15% based on the shroud was conducted using a seventh-order Bezier curve function [30]. A uniform wall temperature of 300 K was applied and analyzed for a  $Re$  of 200,000 for HTC to derive the following expression:

$$Nu = \frac{h_c C}{k}. \quad (2)$$

The NHFR represents a complete assessment of the thermal load at the endwall, which is determined by employing the FCE ( $\eta$ ), the nondimensional metal temperature ( $\phi$ ) value of 1.6 [31], and the HTC, as follows:

$$NHFR = 1 - \frac{h}{h_0} (1 - \eta\phi). \quad (3)$$

The total pressure loss coefficient (TPLC) with coolant blowing ( $P$  is pressure and  $f$  is static) is derived as follows:

$$TPLC = \frac{\frac{\dot{m}_c}{\dot{m}_c + \dot{m}_m} P_{t,cin} + \frac{\dot{m}_c}{\dot{m} + \dot{m}_m} P_{t,m} - P_{t,f}}{P_{t,m} - P_f}. \quad (4)$$

Validation with the experimental  $Nu$  value of 25 at an MFR of 2.5 along the mid-pitch for the contoured endwall [30] shows superior inclination accordance. Moreover, the quantity manifests divergences at locations of the blade leading edge upstream ( $x < 0$ ), which could be attributed to the surface roughness (treated as smooth in simulations). Predictions do not capture an increase in heat transfer, which might be caused by the suction side leg of the HV. The turbulent kinetic energy obtained through measurements could include the contribution of deterministic unsteadiness because of the bimodal nature of the HV. The denser turbulent kinetic energy attained through predictions could be a contributing factor to the thermal exchange gradients. In general, simulation-based forecasting shows superior inclination accordance with the experimental values. Moreover, the quantity manifests divergences at  $x < 0$ . The highest forecasting error is  $<19\%$  in the entire blade passage ( $0 < x/C_{ax} < 0.65 C_{ax}$ ) and  $<1.25\%$  downstream of the blade passage throat ( $x > 0.65 C_{ax}$ ). This forecasting error could be attributed to the experimental surface roughness of the endwall (treated as the smooth surface in CFD simulations) and the

inadequate forecasting of secondary flows at the endwall region. The current simulation method is authentic and can be employed to analyze the impacts of axisymmetric convergent contouring and BR on the film cooling distributions of the endwall and associated phantom cooling, aerodynamic accomplishments, turbine stage efficiency, and thermal exchange of the blade pressure side. Many scientists published the prevalence of peak forecasting error up to 20% concerning contoured endwall and a paramount divergence, particularly in regions with high skew ( $>70^\circ$ ), and adverse pressure gradients downstream of HV detachment and rejoining flow because of appropriate procuring of the multiplex flow physics [30].

The boundary conditions enforced are provided in Table 1. Periodic conditions were allocated for the boundary in the direction of the pitch. The passage entrance of the vane in the computational domain was detected at  $1.2C_{ax}$  upstream of its leading edge. Different coolant flow rates were set at the coolant inlet depending on  $MFR = 0.5-2.5$ . At the inlet of the computational model, the total temperature, total pressure, and mass flow were provided. At the exit, a constant mean pressure was provided. No-slip and adiabatic conditions were allocated for the boundary walls of the plenum and holes of the coolant. The temperatures of the coolant were set as 295–298 K.

Non-axisymmetric endwall contouring based on the shroud is performed using a seventh-order Bezier curve function [32] with 15% perturbation height to span.

### 3. Effect of Endwall Contouring

#### Endwall Heat Transfer

**Axisymmetric contouring with coolant injection.** A higher coolant flow rate noticeably diminishes the thermal load adjacent to the upstream location to the vane leading edge of the contoured endwall at an MFR of 1.5%. With increased coolant MFR, the distribution of the coolant film is highly augmented at the suction side of the airfoil along the direction of the stream in the case of contoured geometry, rather than flat geometry. This phenomenon could be attributed to coolant attachment because of the effect of contouring at the passage downstream, with the endwall scarcely having any impact on the secondary flow. The endwall with the flat geometry exhibits marginally augmented productiveness at the anterior part of the blade leading edge at an MFR of 1.5%.

**Non-axisymmetric contouring.** When non-axisymmetric contouring is attempted, a specific shape, i.e., “S,” results, as convex and concave areas are assigned adjacent to the pressure and suction surfaces, respectively. The original axisymmetric endwall has a zero-perturbation height percent to span. The optimization of

the endwall with respect to the non-axisymmetric shroud led to marked enhanced stage efficiency and output torque of the turbine when the perturbation height was 15%. The endwall optimization with respect to the non-axisymmetric shroud efficiently and extensively enhances the performance of the turbine.

**Pitch-averaged endwall Nusselt number.** The pitch-averaged  $Nu$  values of flat, axisymmetric, and non-axisymmetric contoured endwall shapes at a BR of 1.5 are shown in Figure 4. The endwall thermal load is increased by up to 12.3% and 12.7% in the entire blade passage ( $0 < x < 0.65C_{ax}$ ) and decreased by up to 57.8% and 66.3% in the location downstream to the passage throat of the blade ( $x > 0.65C_{ax}$ ) for the axisymmetric and non-axisymmetric contoured endwalls, respectively. Contouring significantly decreases the endwall thermal load. The reverse flow adjacent to the endwall corner on the suction side migrates farther from the vane surface, as the deviated pressure distribution on the endwall accelerates the flow and progresses the reverse flow core still downstream. At a BR of 1.5 (Figure 4), the endwall heat transfer increases for both the endwall contoured shapes in the location upstream to the passage of the blade ( $x < 0.4C_{ax}$ ) but decreases in the region downstream to the passage throat of the blade ( $x > 0.65C_{ax}$ ).

A prominent interaction between coolant and secondary flow is observed for the geometry of the contoured endwall, which is manifested in the  $Nu$  distribution (Figure 5). The leakage flow arising out of the upstream slot accompanies the trajectory crossed in the middle of the pressure and suction side legs of the HV of the nearby airfoil and progressively fades out across the flow direction of the mainstream. The coolant jet percolation range and scattering within the passage flow toward the mainstream increase with the augmentation of the coolant MFRs by 0.5% to 1.5%. Distinctively, as the coolant momentum flux is elevated, the dissipation rate is also augmented; hence, the powerful association between the flows of the mainstream and coolant in an accumulation region adjacent to the coolant outlet generates an elevated thermal exchange region proliferating with an enhanced MFR. The intensification of the slot-generated coolant vortex disseminating supplementary coolant momentum flux has been accredited to the elevated HTC values in this zone. The coolant vortex is a powerful category of cavity vortex because of coolant inclusion. The augmentation of the regional endwall thermal load due to the coolant jet merger is also noticed in contoured geometry, mainly in the cases where the MFR is 0.5% and 1.0%. However, the zone is relocated further downstream in contrast to the flat endwall geometry. In the case of a contoured endwall geometry at an elevated MFR (1.5%), a higher coolant flow rate remarkably lowers the thermal load adjacent to the upstream zone and the vane leading edge. Notably, with an elevated MFR, greater cooling is

attained adjacent to the location of the inactive leading edge. However, for the case with an MFR of 1.5%, the coolant distribution across the mainstream orientation does not exceed 1.0% because of the prospective coolant lift-off from the endwall. In the case of the contoured endwall, specifically with an elevated coolant MFR, the distribution of the coolant film is outstandingly enhanced in the direction of the stream, as well as all over the airfoils at its suction side, in contrast to the flat endwall. This phenomenon is ascribed to the impact of contouring that assists the coolant in attaching to the endwall substantially downstream of the passage and, at the same time, not critically dominated by the secondary flow.

**Net heat flux reduction.** An augmented NHFR reveals a diminished thermal load on the endwall. An axisymmetric contoured endwall notably enhances the endwall NHFR at an MFR of 1.5%, resulting in a lower endwall thermal load than a flat endwall. At an MFR of  $< 1.0\%$ , NHFR is attained with a diminished thermal exchange, rather than an enhanced film cooling; therefore, NHFR augmentation is not beneficial. At an MFR of 1.5%, a contoured endwall considerably enhances the NHFR (Figure 6) at  $x/C_{ax} < 0.65$  (i.e., up to 5.2% and 20.6% for the axisymmetric and non-axisymmetric contoured endwalls, respectively) with a still elevated value downstream (i.e., up to 20% and 50% for the axisymmetric and non-axisymmetric contoured endwalls, respectively). A non-axisymmetric contoured endwall achieves the highest NHFR at most locations of the endwall, which could be attributed to the enhanced FCE and diminished thermal exchange rates. As the contoured endwall possesses a vast area for cooling, the augmented cooling gained in the passage disappears. At an MFR of  $> 1.625\%$ , although the effect of adiabatic cooling effectiveness augmentation is elevated, the net endwall thermal exchange in the modified area is lower than that in the passage.

The noticeable enhancement in NHFR at the non-axisymmetric contoured endwall (Figure 6) is the result of lowering the passage vortex vigor (by effectively controlling the secondary flow) and flow gradients of the cross-passage, as well as the coolant film capacity in piercing the passage farther till the trailing edge at elevated MFR. The NHFR at the pressure side is mainly the result of a decrease in local HTC. The impact of the distribution of the coolant film is dominant in the direction of the platform on its suction side and to the slot at the stagnation region downstream. An augmented gross  $Nu$  is noticeable with a contoured endwall, and a considerable enhancement in NHFR can be obtained as the FCE is higher in the contoured endwall than in the flat endwall. At an MFR of 1.5%, the thermal load of a contoured endwall is elevated because the coolant film unites along the surface due to contouring; by contrast, jet lift-off occurs with the flat endwall. A non-axisymmetric contoured endwall considerably augments the endwall NHFR (averaged crosswise at the direction

of length) at an MFR of 1.5% (Figure 6). Hence, contoured geometries can lower the endwall heat load than a flat geometry.

**Aerodynamic performance.** Figure 7 shows the TPLC derived with the mean mass flow at an MFR of 0% to 2.5% and  $x/C_{ax}$  of 1.25 in the passage of contoured and flat endwalls. The non-axisymmetric contoured passage of the endwall exhibited augmented aerodynamic performance with inferior TPLC standards than the axisymmetric contoured endwall, as well as the flat endwall, at the range of MFR used in the current investigation. At an MFR of 1.5%, the contoured endwalls (i.e., axisymmetric and non-axisymmetric) showed better aerodynamic performance, whereas the flat endwall showed an inferior aerodynamic performance compared with that at lower MFR values. When the MFRs, as well as the momentum fluxes, are elevated with coolant injection, supplementary vortices develop at the upstream location and aerodynamic losses are elevated. The TPLC attained with the average mass flow of every passage manifested an orientation similar to that of MFR. As the MFR increases, the TPLC first increases, halts in the interim, decreases at a certain MFR range, and then increases again. At lower MFR, passages experience unfavorable aerodynamic losses compared

with those at higher MFR, disregarding the MFR range with hot gas ingestion. The minor TPLC attained with the average mass flow is attributed to the diminished vortices as a result of coolant injection at the upstream leading edge. When the momentum fluxes and MFRs are augmented with coolant injection, supplementary vortices progress over the upstream position, and aerodynamic drops are augmented.

When coolant injection is not considered, the pressure loss distribution showed a prominent impact on the overall pressure loss. At the juncture of the coolant injection inclusion, the wake zone toward the pitch direction was sustained and nearly fixed at its suction side in contrast to that at its pressure side. This irregular wake region development results from the association between the injected coolant and the mainstream. At the juncture of sufficiently injected coolant, the gross pressure loss behind the slot exit is reduced, and the momentum of the coolant jet remains high. By contrast, the gross pressure loss behind the solid location is elevated, with the coolant jet diffused and its momentum weakened. Hence, the gross pressure loss is elevated in the cutback, as well as the central slots, of the injection.

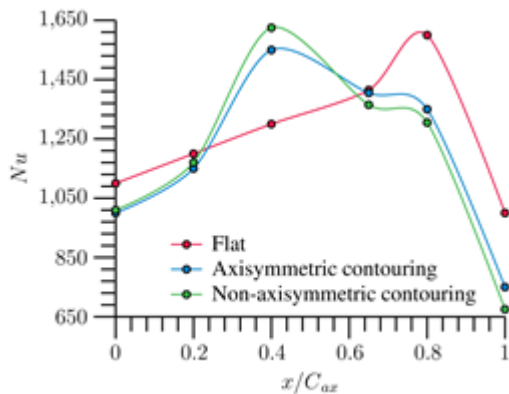


Figure 4. Pitch-averaged Endwall  $Nu$  for Flat and Contoured Endwalls at a BR of 1.5

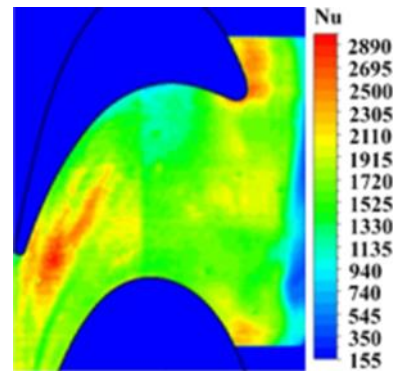


Figure 5. Cloud Map of Endwall  $Nu$  Distribution with an MFR of 1.5% for Contoured Endwall

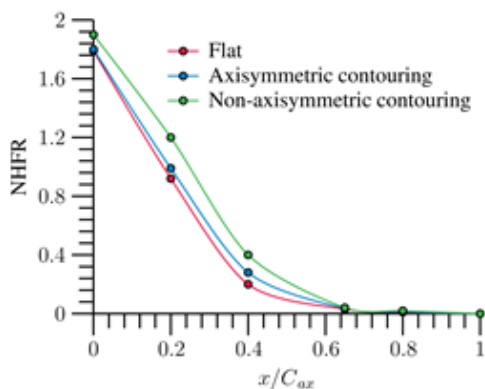


Figure 6. Comparison of NHFR in Flat and Contoured Endwalls at an MFR of 1.5

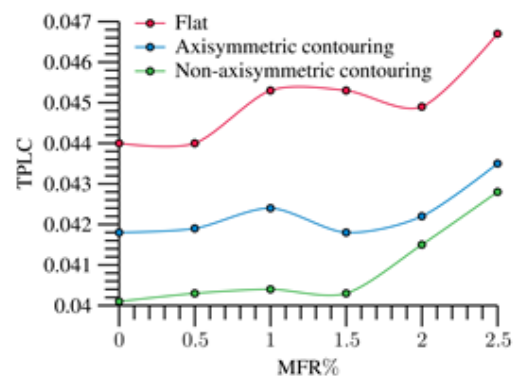


Figure 7. TPLC at an MFR of 0% to 2.5% and  $x/C_{ax}$  of 1.25 in the Passage of Flat and Contoured Endwalls

## 4. Conclusion

A detailed numerical investigation of endwall heat transfer, NHFR, and mass-averaged TPLC (aerodynamic performance) is presented using turbine vane endwall with flat, axisymmetric, and non-axisymmetric contoured geometries and realizable  $k-\epsilon$  turbulence model. These characteristics are comparatively analyzed for three endwall contoured shapes at different MFRs. The major conclusions are as follows:

1. The endwall boundary layer is unaffected by the small passage vortex that emerged, which reduced the thermal exchange in the passage of contoured endwalls compared with that of flat endwalls.
2. The non-axisymmetric contoured geometry developed based on a shroud with 15% perturbation height to span showed better thermal load reduction at the endwall than the axisymmetric contoured and flat geometries.
3. The axisymmetric contoured geometry outperformed the flat geometry in lowering the endwall heat load.
4. The present numerical method based on the realizable  $k-\epsilon$  turbulence model can accurately predict endwall thermal load distributions, NHFR, and mass-averaged TPLC.
5. The contoured endwalls outperform the flat geometry based on NHFR, especially near the conventional hot-spot regions at an MFR of 1.5%, with better coolant coverage for non-axisymmetric contoured endwalls.
6. The mass-averaged TPLC shows a significant reduction with the introduction of contoured endwalls with the best elevated aerodynamic performance at an MFR of 1.5% for non-axisymmetric contoured endwalls.
7. The non-axisymmetric and axisymmetric convergent contouring is beneficial for the endwall NHFR and vane passage aerodynamic performance, with the non-axisymmetric contouring being the best.

Improving endwall heat exchange prediction appears to be the prospective major barrier in augmenting turbine performance and persistence through perfect thermal designs. Thus, the integrated impacts of the appropriate axisymmetric convergent or non-axisymmetric endwall contouring, as well as the optimum BR, must be evaluated during the design activity of advanced strategies of endwall cooling.

## References

[1] Y. Liu, Y. Rao, L. Yang, *Int. J. Therm. Sci.* 153 (2020) 106337.  
 [2] L. Wang, X. Li, J. Ren, H. Jiang, *Int. J. Therm. Sci.* 149 (2020) 106176.  
 [3] M. Thomas, T. Povey, *P. I. Mech. Eng. G-J. Aer.* 231/14 (2017) 2689.  
 [4] Z. Cao, C. Wang, J. Zhao, X. Hao, Z. Song, B. Liu,

*Int. J. Turbo Jet Eng.* 40(s1) (2023) s621.  
 [5] T.J. Praisner, E. Allen-Bradley, E.A. Grover, D.C. Knezevici, S.A. Sjolander, *J. Turbomach.* 135/6 (2013) 061006.  
 [6] S.P. Lynch, Ph.D Thesis, Virginia Polytech Institute and State University, Virginia, USA, 2011.  
 [7] Z. Robison, Ph.D Thesis, New Mexico State University, New Mexico, 2022.  
 [8] J. Li, X. Yan, K. He, *J. Turbomach.* 142/5 (2020) 051006.  
 [9] S. Hussain, J. Liu, B. Sunden, *Appl. Therm. Eng.* 168 (2020) 114844.  
 [10] L. Song, Z. Guo, J. Li, Z. Feng, *J. Propuls. Power.* 34/1 (2018) 234.  
 [11] L. Song, P. Zhu, J. Li, Z. Feng, *Appl. Therm. Eng.* 110 (2017) 504.  
 [12] S.P. Lynch, K.A. Thole, A. Kohli, C. Lehane, *J. Turbomach.* 133/4 (2011) 041003.  
 [13] T.W. Zimmermann, O. Curkovic, M. Wirsum, A. Fowler, K. Patel, *J. Turbomach.* 139 (2017) 061007.  
 [14] W. Duan, W. Qiao, Z. Wei, J. Liu, H. Cheng, *Proceedings of ASME Turbo Expo, Oslo, Norway, 2018*, p.76159.  
 [15] A. Thrift, K.A. Thole, S. Hada, *J. Turbomach.* 133/4 (2011a) 041008.  
 [16] A. Thrift, K.A. Thole, S. Hada, *J. Turbomach.* 133/4 (2011b) 041007.  
 [17] J.C. Han, *J. Therm. Sci. Eng. Appl.* 5/2 (2016) 021007.  
 [18] Z. Guo, H. Bu, L. Song, *Aerosp. Sci. Technol.* 85 (2019) 429.  
 [19] J. Bergh, G. Snedden, D. Dunn, *J. Turbomach.* 142/4 (2020) 041006.  
 [20] P. Chen, K. Zhao, X. Li, J. Ren, H. Jiang, *Int. J. Therm. Sci.* 161 (2021a) 106689.  
 [21] P. Chen, X. Li, J. Ren, H. Jiang, *Int. J. Gas Turbine Propulsion Power Syst.* 12/1 (2021) 1.  
 [22] K.S. Arjun, P.S. Tide, N. Biju, *Makara J. Tech.* 27/2 (2023) 68.  
 [23] K. S. Arjun, P. S. Tide, N. Biju, *J. Harbin Inst. Tech.* 31/2 (2024) 80.  
 [24] K.S. Arjun, P.S. Tide, N. Biju, *J. Harbin Inst. Tech.* (2023).  
 [25] K.S. Arjun, P.S. Tide, *Sci. Tech. J. Inf. Technol. Mech. Opt.* 23/6 (2023) 1223.  
 [26] K.V. Panchal, S.Abraham, S.V. Ekkad, W.F. Ng, A.S. Lohaus, M.E. Crawford, *J. Turbomach.* 139 (2017) 011009.  
 [27] D.G. Knost, MS Thesis, Virginia Polytech Institute and State University, Virginia, USA, 2003.  
 [28] S. Hada, K.A., Thole, *J. Turbomach.* 133 (2011) 011024.  
 [29] K. Du, J. Li, *Int. J. Heat Mass Tran.* 98 (2016) 768.  
 [30] B. Bai, Z. Li, J. Li, S. Mao, W.F. Ng, *J. Eng. Gas Turb. Power.* 144/2 (2022) 021020.  
 [31] G.J. Zhao, *J. Propuls. Technol.* 35/5 (2014) 597.  
 [32] S.P. Lynch, K.A. Thole, *J. Turbomach.* 139 (2017) 051002.